Materials Science & Engineering A 931 (2025) 148235

Contents lists available at ScienceDirect

Materials Science & Engineering A

journal homepage: www.elsevier.com/locate/msea

Yield of cyclic vs heat-and-hold induction sintering on the mechanical behaviour of the low-cost Ti-5Fe alloy

L. Bolzoni [a,*], V. Roduit [a,b], E. Carreno-Morelli [b], F. Yang [a], S. Raynova [a]

[a] School of Engineering, The University of Waikato, Hamilton, 3240, New Zealand
[b] University of Applied Sciences and Arts Western Switzerland, 1950, Sion, Switzerland

ARTICLE INFO

Keywords:
Titanium alloys
Powder metallurgy
Blended elemental
Homogeneous microstructure
Mechanical properties

ABSTRACT

The high cost of Ti alloys is hindering their industrial implementation and, therefore, the quest for low-cost Ti alloys entails lowering the intrinsic cost using cheaper alloying elements and developing more efficient manufacturing methods. In this study, the yield of manufacturing the novel low-cost Ti-5Fe alloy via heat-and-hold and cyclic induction sintering around the allotropic α→β phase transformation was compared as the latter is expected to enhance densification. It is demonstrated that induction sintering is extremely efficient due to its characteristic high heating rates and simultaneously permits to obtain homogenous chemical compositions at low homologous sintering temperatures. Cyclic sintering yields faster sintering kinetics, which results in higher densification with respect to heat-and-hold, achieving uniform residual porosity distributions within the microstructure, comparable relative density, and on average smaller and more spherical pores. Consequently, higher strength but not necessarily higher ductility is obtained for the cyclic sintered Ti-5Fe alloy as the failure mode entails crack propagation through irregularly shaped pores.

1. Introduction

Titanium (Ti) alloys are characterised by a remarkable combination of properties including the highest specific strength amongst structural metals, low density, relatively low Young modulus, paramagnetism, excellent corrosion resistance, and biocompatibility [1,2]. Because of such characteristics, Ti alloys are ideally suited for a wide range of engineering applications but they are generally only used in high demanding sector like aerospace, petrochemical, and bio-engineering/health care [3,4]. This is because of the much higher cost of Ti alloys in comparison to competitors metals like Al [5,6], where the high cost is the accumulation of several factors derived from the need of using specialised and costly processes to extract and manufacture Ti alloys components primarily due to its great affinity for oxygen. Amongst Ti alloys, the α+β alloys are the most widely studied and applied due to the fact that their duplex microstructure entails the best compromise between strength and toughness and their performance can easily be tailored by changing the duplex lamellar, equiaxed, or bimodal microstructure by means of manufacturing and heat treatment procedures [7]. Ti-6Al-4V is the most well studied Ti alloy and, after approximately 80 years from its discovery, still accounts for more than half of the overall annual Ti alloys production [8]. In recent years, scientific interest has risen for lowering the intrinsic cost of Ti alloys by using cheaper alloying elements, in particular with the aim of avoiding V as a β stabiliser [9,10]. In Ti alloys, β stabiliser are commonly divided between isomorphous (e.g., V, Nb) and eutectoid (e.g., Fe, Mn) elements depending on their maximum solubility in the Ti lattice. Amongst eutectoid β stabiliser, Fe is one of the most promising alloying elements for designing and developing low-cost Ti alloys due to its β stabilisation power, which is generally taken into account by using the molybdenum equivalent concept [11], high diffusivity, and low cost [12]. These advantages are further accrued when manufacturing Ti alloys via powder metallurgy (PM) as ferrous powders have been optimised over the years by the PM industry.

In actuality, PM has several advantages when it comes to the manufacturing of Ti alloys with respect to the classical wrought metallurgy route. Specifically, PM methods are mainly solid-state processes, which is advantageous because they are more energy efficient (i.e., environmentally friendly), limit the reactivity of Ti at high temperatures, and prevents the sedimentation of heavy alloying elements, a common problem during casting [13]. Moreover, PM allows preventing the formation of brittle TiFe-based intermetallic compounds due to the

* Corresponding author.
E-mail address: bolzoni.leandro@gmail.com (L. Bolzoni).

https://doi.org/10.1016/j.msea.2025.148235
Received 19 December 2024; Received in revised form 13 March 2025; Accepted 17 March 2025
Available online 18 March 2025

sluggish phase transformation kinetics. PM methods are also net- or near-net-shape processes meaning that the material yield is high (>90 %), the number of operations is reduced (i.e., lower cost), and the amount of machining required is limited. The latter is generally problematic due to the low thermal conductivity of Ti, which is classified as a difficult-to-machine metal. When it comes to PM Ti-Fe alloys, we previously demonstrated that the conventional PM manufacturing (i.e., sintering at high temperatures) of the Ti-5Fe alloy yields a lamellar α+β microstructure and comparable properties to those of the Ti-6Al-4V can be achieved at lower cost. Specifically, we clarified the effects of induction [14], vacuum [15], and microwave [16] sintering without and with subsequent post-sintering thermomechanical processing like forging [17] and extrusion [18,19] on the microstructural features and mechanical performance. Along these lines, Germain Careau et al. [20] investigated direct powder forging where the blended elemental powder blend is encapsulated prior to its thermomechanical processing, demonstrating the achievement of fully dense, alloys although the interaction between the powder blend and the 316L stainless container proved to be an issue. Germain Careau et al. [21] have recently also worked on developing a gas atomised prealloyed Ti-5Fe powder for additive manufacturing. Want et al. [22] actually used laser *in-situ* alloying additive manufacturing starting from a blended elemental powder blend to manufacture the Ti-5Fe alloy and studied its mechanical and *in-vitro* biocompatibility performance, as targeting biomedical applications. Despite of their intrinsic advantages, these advanced manufacturing techniques are impaired by long processing times, and pressureless sintering, especially if it can be done very fast, remains the most cost-effective PM method.

Amongst PM pressureless sintering techniques, induction sintering is characterised by very short processing cycles as a result of the extremely high achievable heating rates, which allow to shorten the sintering time from hours to minutes [23]. This is possible because the process generates heat by inducing a high-frequency electric current inside the conductive material. Initially, heat is generated by the electromagnetic field induced by the alternating current passing through the conductive material, which generates eddy currents and internal resistant heating. Subsequently, heat propagates through the entire alloy via conduction resulting in an overall homogeneous, faster, more efficient, and more reliable heating. The outwards fast heating induces fracturing of the superficial oxide layer present in the powder particles due to significant differences in the coefficient of thermal expansion, allowing metal-to-metal interaction and quick material transfer along neighbouring powder particles. Previous research has shown that cyclic phase transformation increases the sintering rate, leading to improved powder densification [24], by enhancing the sintering driving force due to the difference in the free energy of the two phases involved as this results in a gradient in the concentration of vacancies [25]. German [26] reported that the α→β transformation in Ti provides strain, defects, and interfaces that accelerate densification in the 800–1100 °C temperature range. Although induction sintering is ideally placed to perform cyclic sintering [27], this has not been exploited and to the best knowledge of the authors there are no studies in literature about induction cyclic sintering as previous reports are only available for conventional sintering (i.e., heating rate 10 °C/s) [28], hot pressing [29], and spark plasma sintering [30].

The aim of this study is, therefore, to quantify the yield of cyclic induction sintering as compared to the classical heat-and-hold sintering for the manufacturing of the low-cost Ti-5Fe alloy. For the sake of comparison and to minimise the sintering cost, low homologous sintering temperatures (primality between 850 °C and 950 °C) were employed; although the effect of a final increment to a high classical sintering temperature for Ti (i.e., 1200 °C) was also investigated. The effectiveness of cyclic sintering was assessed by quantifying the achievable densification and through an in-depth analysis of the features of the resultant pore structure. These, along with the results of microstructural and phase characterisations, where used to clarify their effects on the obtained mechanical behaviour and to identify the feature that does have the highest impact on them.

2. Experimental procedure

The raw materials used to create the Ti-5Fe alloy were elemental hydride-dehydride (HDH) Ti powder (particle size <75 μm, purity 99.4 %, and oxygen 0.25 wt%; data as per supplier specifications) and carbonyl Fe powder (particle size <10 μm, purity 99.5 %, and oxygen 0.32 wt%; data as per supplier specifications). Fig. 1 shows the micrographs of the raw materials where it can be seen that the HDH powder has an irregular morphology whilst the Fe powder is characterised by a spherical morphology.

In order to obtain a homogeneous powder blend, the correct amount of powders was mixed in a V-shape blender operated at 60 Hz for 30 min. The Ti-5Fe alloy powder blends were subsequently cold uniaxially pressed into 40 mm diameter cylindrical samples using a 100 Ton press applying a pressure of 600 MPa resulting in an approximate height of 20 mm. Consolidation of the samples was done by means of induction sintering performed in an in-house made experimental setup consisting of a glove box chamber equipped with a copper induction coil externally connected to a high frequency induction heating power supply unit [23]. Prior to sintering, the chamber was purged three times and subsequently Argon was continuously run to maintain the oxygen level below 200 ppm. Induction sintering was done using five different thermal cycles, which are summarised in Table 1, to assess the effectiveness of cyclic sintering in comparison to holding the alloy at the sintering temperature. Cycle 1 entailed heating up to 950 °C, let the sample cool down to 850 °C followed by heating and cooling between these two temperatures 5 times. In cycle 2 to 4 the samples were heated up to the maximum temperature (850 °C, 900 °C, and 950 °C, respectively) and kept at temperature for 8 min. Cycle 5 is the same of cycle 1 but the last cooling down to 850 °C was followed by heating the samples up to 1200 °C, instead of 950 °C prior to the final cooling. It is worth mentioning that the average heating rate up to 800 °C is approximately 3.85 °C/s (i.e., ~230 °C/min), but the actual rate is affected by the green density of the compact, and cooling was done by switching off the power (i.e., natural cooling). From Table 1 it can be seen that the average total processing time for the cyclic sintering cycles is around 20 min whilst that of the conventional heat-and-hold cycle is approximately 13 min.

The theoretical density (ρ_t) of the Ti-5Fe alloy (i.e., 4.67 g/cm^3) was calculated by means of the rule of mixture using the available density of Ti (i.e., 4.51 g/cm^3) and Fe (i.e., 7.80 g/cm^3). The density of the green compacts (ρ_g) was computed by dividing the mass and the volume of the specimens. The density of the sintered samples (ρ_s) was quantified by means of triplicate water displacement measurements. Quantification of the effectiveness of the sintering cycle was done using the density gain between the green and sintered samples as well as by means of the densification parameter, which was calculated by means of Eq. (1):

$$\Psi = (\rho_s - \rho_g) / (\rho_t - \rho_g) * 100 \quad \text{Eq. 1}$$

The preparation of the samples for microstructural analysis entailed grinding with SiC papers followed by polishing and, if needed, final chemical etching using a Kroll reagent (2 % HF and 6 % HNO_3). An Olympus BX53M optical microscope was used to analyse the distribution of the porosity where 25 per sample images were taken to determine its features through image analysis via the ImageJ software. This included the total amount of pores, their size distribution using the Feret diameter, and their circularity where a value of 1 means a perfectly spherical pore. A Hitachi Regulus 8230 scanning electron microscope (SEM) was used to further analyse the microstructure and determine the homogeneity of the distribution of Fe by means of EDS. An Instron 33R-4204 tester was used to quantify the tensile behaviour of the samples using a crosshead speed of 0.1 mm/min. The elongation was measured by means of a 10 mm mechanical extensometer. A minimum of five samples

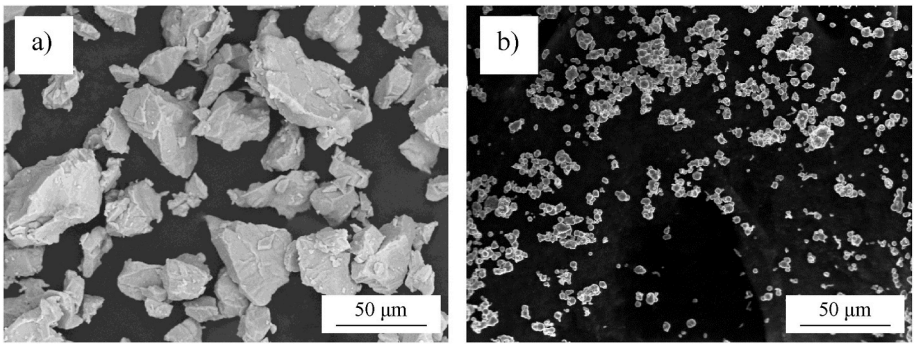

Fig. 1. Micrographs of the raw powders: a) HDH Ti, and b) carbonyl Fe.

Table 1
Thermal cycles used to induction sinter the Ti-5Fe alloy.

Cycle	Description	Label	Total time
1	Heating to 950 °C followed by cooling to 850 °C, cycled 5 times	850-950 °C x 5 times	19 min 45 s
2	Heating to 850 °C followed by 8 min dwell at maximum temperature	850 °C - 8 min	13 min 2 s
3	Heating to 900 °C followed by 8 min dwell at maximum temperature	900 °C - 8 min	12 min 23 s
4	Heating to 950 °C followed by 8 min dwell at maximum temperature	950 °C - 8 min	13 min 37 s
5	Heating to 950 °C followed by cooling to 850 °C, cycled 4 times, plus heating to 1200 °C	850-950 °C x 4 times +1200 °C	22 min 4 s

per sintering condition was tested. Fractographic analysis of the tensile samples was performed at the SEM. A LECO LM700 hardness tester was used for measuring the Vickers microhardness ($HV_{0.1}$) by performing at least seven different measurements.

3. Results

The values of the green density and sintered density of the Ti-5Fe samples are shown in Fig. 2 where it can be seen that there are minor variations in terms of the specific green density (3.77–3.95 g/cm^3) and sintered density (4.11–4.26 g/cm^3) of each sample, but there is not a common trend. However, from the analysis of the density gain and densification, which take into account the actual effectiveness of the sintering cycle, it is found that higher values are always achieved when using cyclic sintering with respect to heat-and-hold. For the latter, both density gain (5.3 → 5.9 %) and densification (30.6 → 34.4 %) monotonically increase with the sintering temperature. A deeper analysis of the correlation between the different aspects of the physical properties and the processing parameters yields that the densification parameter best correlates with the total sintering cycle time (Fig. 2c).

Fig. 3 shows an overview of the pore structure of the Ti-5Fe alloy cyclic sintered 5 times between 850 °C and 950 °C (i.e., cycle 1) where it

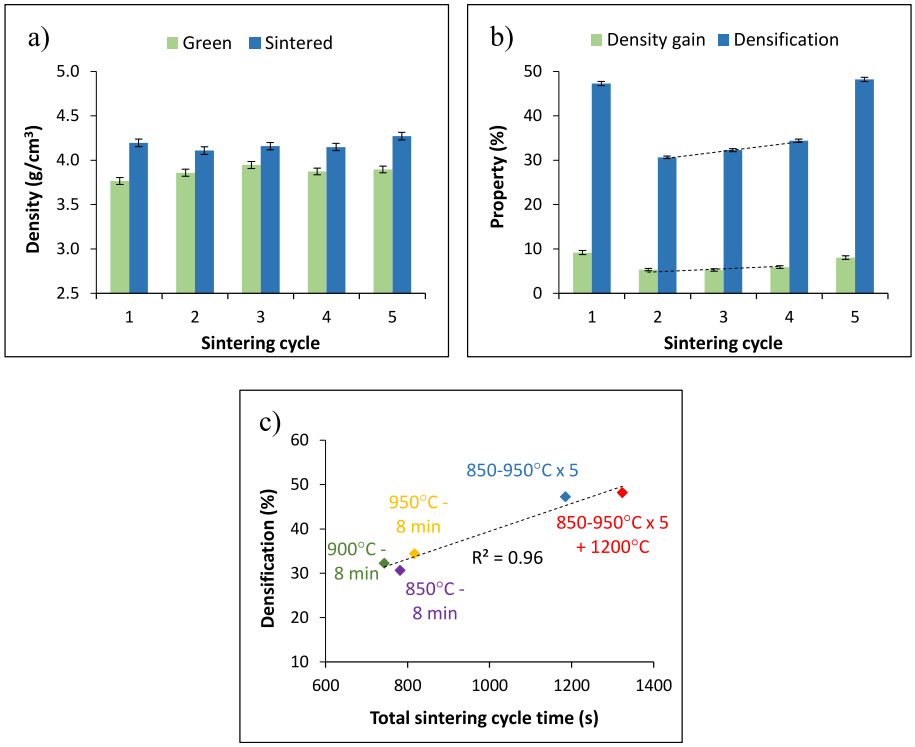

Fig. 2. Values of the physical properties of the induction sintered Ti-5Fe samples: a) green and sintered density, b) density gain and densification, and c) correlation between densification and total sintering cycle time. (For interpretation of the references to colour in this figure legend, the reader is referred to the Web version of this article.)

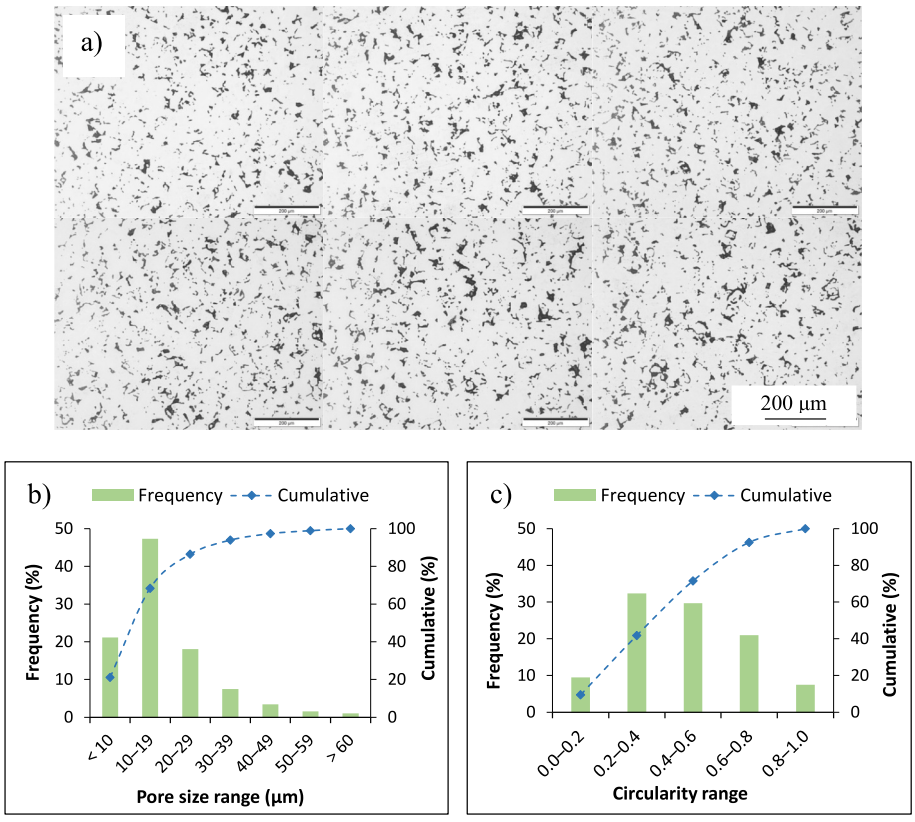

Fig. 3. Results of the characterisation of the porosity of the Ti-5Fe alloy cyclic sintered 5 times between 850 and 950 °C (i.e., cycle 1): a) overview of the pore structure, b) pore size distribution, and c) pores circularity distribution.

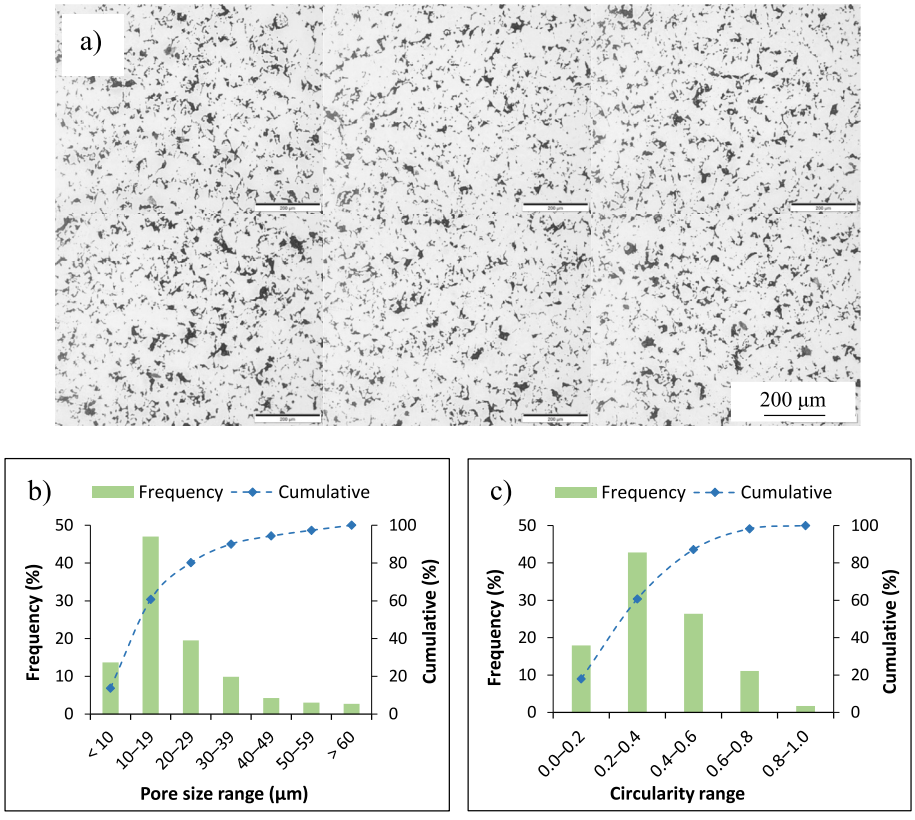

Fig. 4. Results of the characterisation of the porosity of the Ti-5Fe alloy sintered at 850 °C for 8 min (i.e., cycle 2): a) overview of the pore structure, b) pore size distribution, and c) pores circularity distribution.

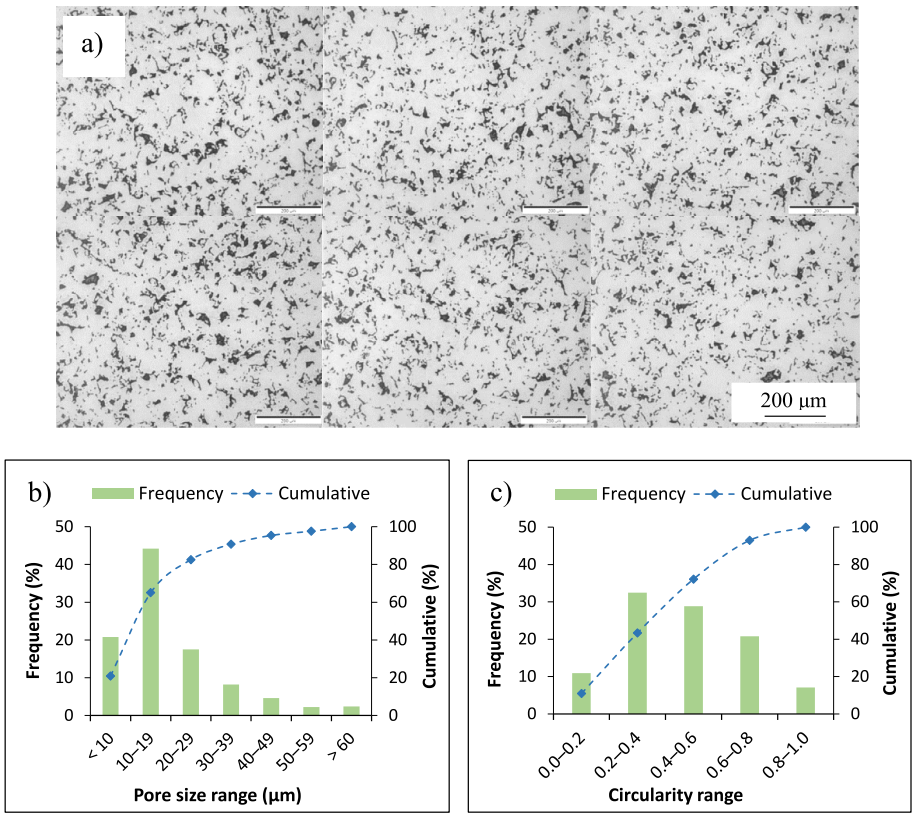

Fig. 5. Results of the characterisation of the porosity of the Ti-5Fe alloy sintered at 900 °C for 8 min (i.e., cycle 3): a) overview of the pore structure, b) pore size distribution, and c) pores circularity distribution.

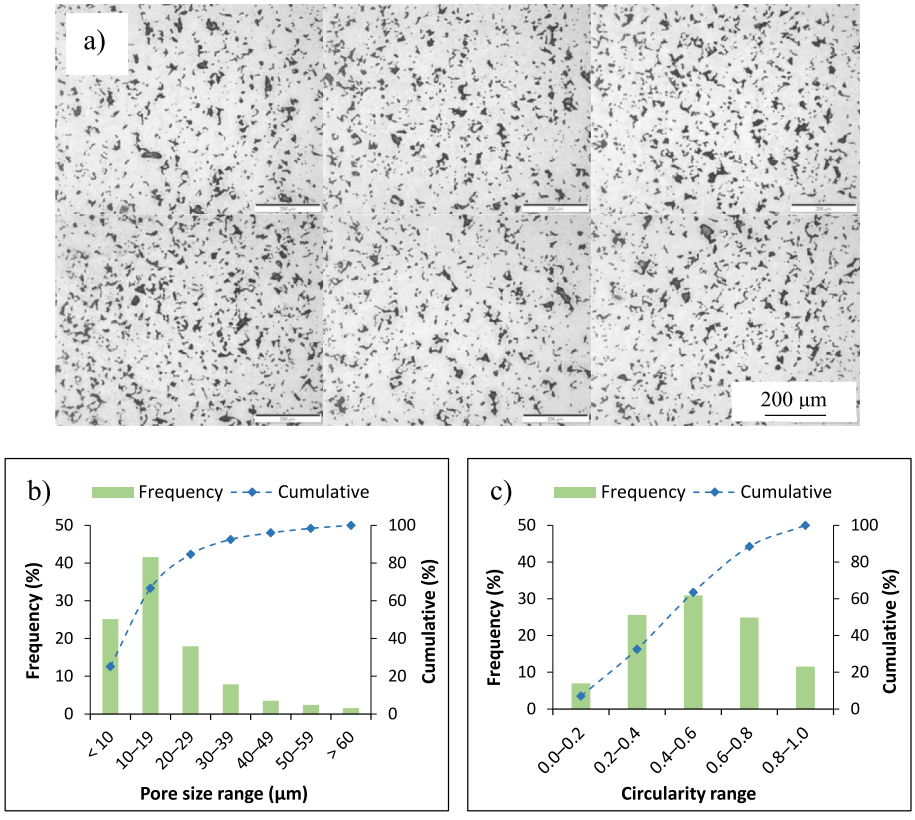

Fig. 6. Results of the characterisation of the porosity of the Ti-5Fe alloy sintered at 950 °C for 8 min (i.e., cycle 4): a) overview of the pore structure, b) pore size distribution, and c) pores circularity distribution.

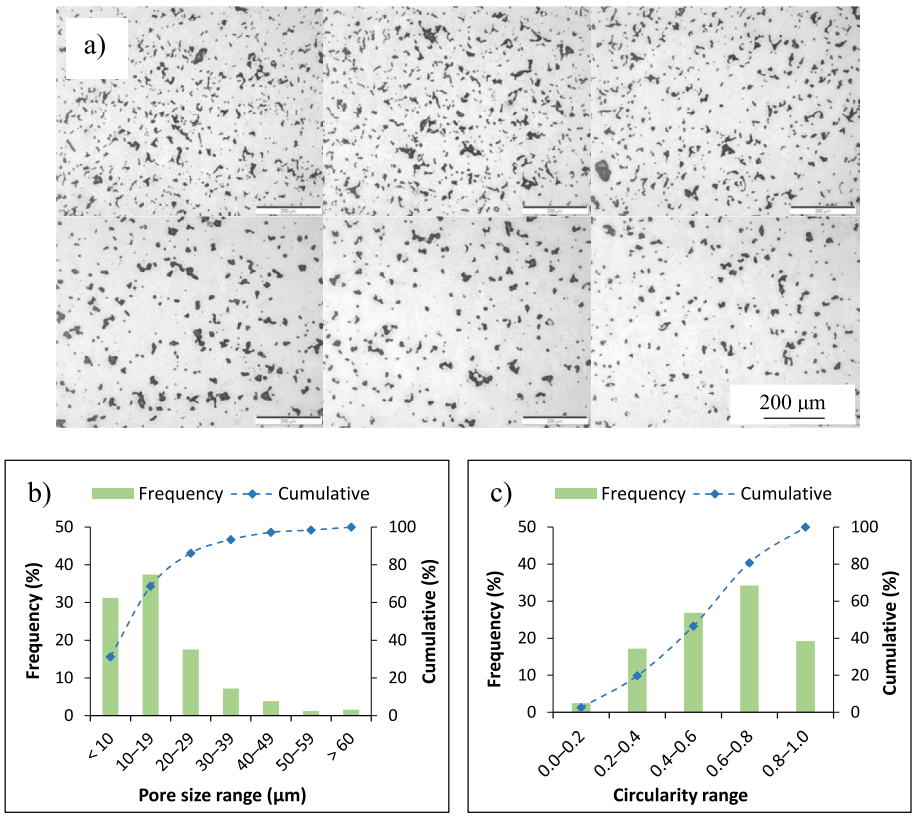

Fig. 7. Results of the characterisation of the porosity of the Ti-5Fe alloy cyclic sintered 4 times between 850 and 950 °C followed by final heating to 1200 °C (i.e., cycle 5): a) overview of the pore structure, b) pore size distribution, and c) pores circularity distribution.

can be seen that a homogeneous distribution of the residual porosity is present in the alloy. The analysis of the features of the pores yields that both the pore size distribution and circularity are characterised by a normal distribution. The majority of the residual pores (i.e., 47.3 %) have a size between 10 µm and 19 µm with 6.1 % of them being larger than 40 µm (Fig. 3b), and the cumulative pore size distribution has a parabolic increasing trend. In the case of the circularity (Figs. 3c), 32 % of the pores are characterised by a value between 0.2 and 0.4 with 7.5 % of them having a value between 0.8 and 1.0, indicating that the morphology of the pores is mainly irregular. It is worth noticing that the cumulative circularity distribution has an almost linear increase rather than a parabolic one.

From the results of the analysis of the pore structure of the Ti-5Fe alloy induction sintered at 850 °C with the classical heat-and-hold procedure (i.e., cycle 2), Fig. 4 shows a homogenous distribution of the residual pores throughout the microstructure. The primary differences in terms of pore size distribution compared to the Ti-5Fe alloy cyclic sintered (Fig. 3) are that the number of pores lower than 10 µm is smaller and the overall number of pores bigger than 40 µm is higher (i.e., 10.0 %). In term of circularity (Fig. 5c), 42.8 % of the pores have a value between 0.2 and 0.4, only 1.7 % of them have a value higher than 0.8, and the increase of the cumulative circularity distribution is parabolic. This indicates that the sintering cycle 2 does not only lead to a lower densification (Fig. 2), but also to on average larger pore size with a greater number of them having an irregular morphology.

Increasing the induction sintering temperature to 900 °C (i.e., cycle 3) does not significantly change the pore size distribution if not that the number of pores smaller than 10 µm is slightly greater but 9.3 % of the pores are still larger than 40 µm (Fig. 5b). The analysis of the circularity of the pores present in the Ti-5Fe alloy induction sintered at 900 °C for 8 min (Fig. 5c) yields comparable results to that of the alloy cyclic sintered between 850 °C and 950 °C (Fig. 3).

In the case of the Ti-5Fe alloy induction sintered at 950 °C for 8 min (i.e., cycle 4) a uniform distribution of the residual pores in the microstructure is found (Fig. 6). The overall distribution of the pore size is similar to previous cases but slightly shifted towards lower values with 7.5 % of the pores having a size larger than 40 µm (Fig. 6b). The most remarkable change is in terms of circularity of the residual pores as the normal distribution is now centred around 0.4–0.6 rather than 0.2–0.4 and the percentage of pores with a circularity value greater than 0.8 is 11.6 % (Fig. 6c). This indicates that a greater number of pores tend to have a more spherical morphology. As a consequence, the circularity distribution cumulative trend is almost linear rather than parabolic.

A slightly less uniform distribution of the pores is obtained in the Ti-5Fe alloy cyclic sintered 5 times between 850 and 950 °C followed by final heating to 1200 °C (i.e., cycle 5) as visible from the representative micrographs of Fig. 7. The number of pores smaller than 10 µm is greater (i.e., 31.2 %), that of pores larger than 40 µm is smaller (i.e., 6.6 %), and pores are much more spherical in shape with 19.2 % of them having a circularity value greater than 0.8.

Fig. 8 shows representative micrographs of the induction sintered Ti-5Fe samples where it can be seen that all the materials are characterised by a lamellar microstructure [31] composed of α+β lamellae enclosed within prior β grains of similar size of approximately 70 µm, which is compatible with the maximum particle size (i.e., 75 µm) of the starting HDH Ti powder. The size and distribution of lamellae (Fig. 8c) is comparable amongst the different induction sintered Ti-5Fe samples, with an average α lath width of 1.53 ± 0.16 µm, although there are minor differences depending on the actual sintering cycle. Microstructural analysis as well as elemental EDS chemical analysis confirm the homogeneity of the composition of induction sintered Ti-5Fe samples regardless of the actual sintering cycle. As Fe is a β stabiliser with limited solubility in the α phase, it can be seen that the average amount of Fe dissolved into the β phase is higher with respect to that of the α phase (Fig. 8f) but the average composition quantified by means of EDS is coherent with the expected nominal composition of 5 wt% of Fe.

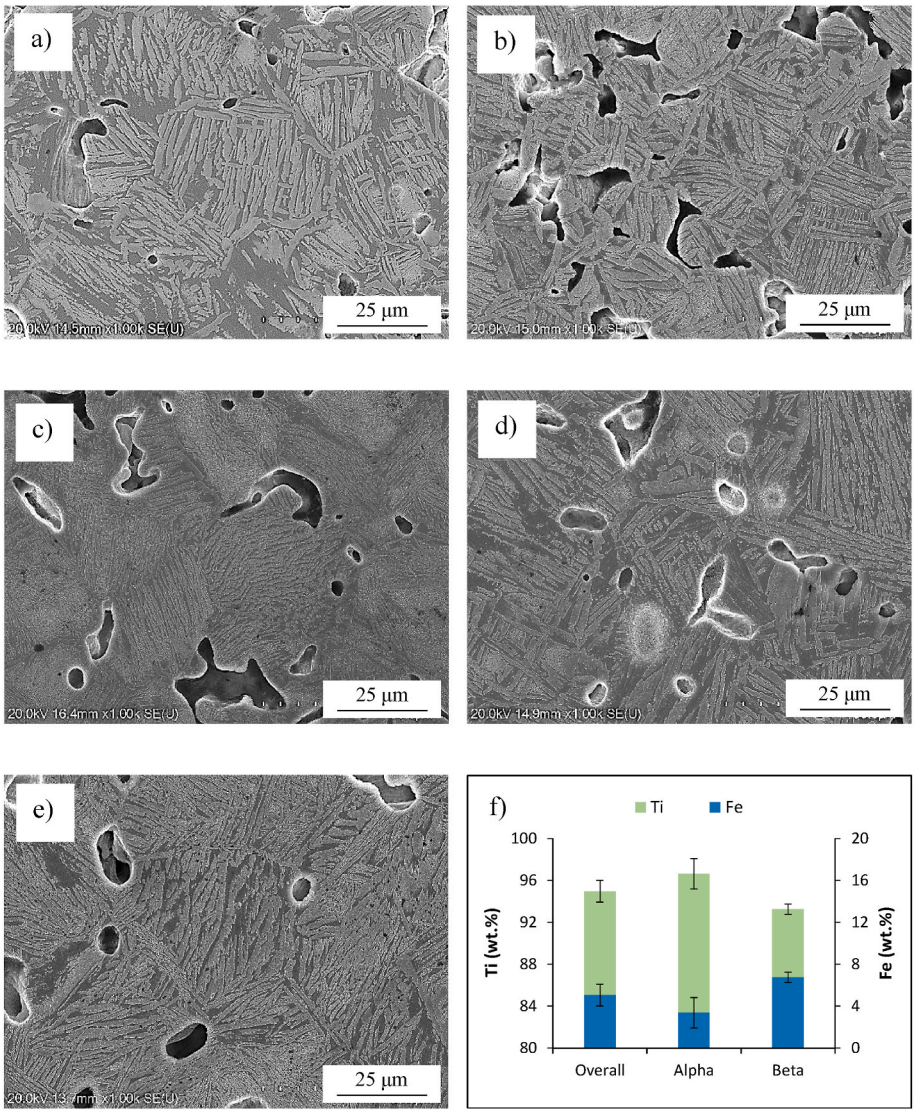

Fig. 8. Microstructural analysis of the induction sintered Ti-5Fe samples: a) cycle 1: 850-950 °C x 5 times, b) cycle 2: 850 °C - 8 min, c) cycle 3: 900 °C - 8 min, d) cycle 4: 950 °C - 8 min, e) cycle 5: 850-950 °C x 4 times +1200 °C, and f) average EDS composition.

The results of the XRD characterisation performed on the induction sintered Ti-5Fe samples are displayed in Fig. 9 showing that both the α and β phases where detected and they were the only phases present in the sintered alloys. This confirm that complete dissolution of the Fe powder particles within the Ti matrix occurred as well as the fact that no intermetallic phases (i.e., TiFe as per the Ti-Fe binary phase diagram [32]) do precipitate upon cooling from the sintering temperature.

Fig. 10 shows representative stress vs. strain curves of the induction sintered Ti-5Fe samples and the associated fractographic analysis results. It can be seen that the induction sintered Ti-5Fe samples are primarily characterised by an elastic response when uniaxially loaded without much plastic deformation if not in the alloys sintered using cycle 4 and cycle 5. Therefore, the latter two are the only one where the yield stress could actually be identified. Although there are minor variations, the induction sintered Ti-5Fe samples are characterised by similar Young modulus. The results of the analysis of the fracture surface of the tensile tested samples is coherent with their mechanical behaviour as rough fracture surfaces, where the alloy primarily failed intergranularly through the interconnection of irregularly shaped pores [33], were found. From the high magnification insets, it is found that plastically deformed ductile dimples are present in between prior β grains where the amount of ductile area increases with the induction sintering temperatures and their number is higher for the cyclic induction sintered Ti-5Fe samples.

4. Discussion

In this study cyclic induction sintering was compared to the standard heat-and-hold sintering procedure to analyse its yield on the properties of the low-cost Ti-5Fe alloy produced by means of the blended elemental approach using HDH Ti and carbonyl Fe powders as raw materials (Fig. 1). The first thing that this study confirms is that induction sintering is characterised by an extremely high heating rate, or short sintering cycle, with respect to the conventional vacuum sintering commonly used to sintered Ti alloys. The average heating rate of 3.85 °C/s of the Ti-5Fe samples, which have an average relative green density of 82.6 ± 1.2 %, agrees with previous reports on the effect of the relative green density on the induction sintering heating rate [23]. The analysis of the physical properties of the induction sintered Ti-5Fe samples shows that there are both variations in the green and sintered density and, consequently, no common trend is found. This is due to the effect of the intrinsic variability of the shaping of the powder blends via uniaxial pressing and the knock-on effect on the response to the induction heating process. Nonetheless, the analysis of the density gain

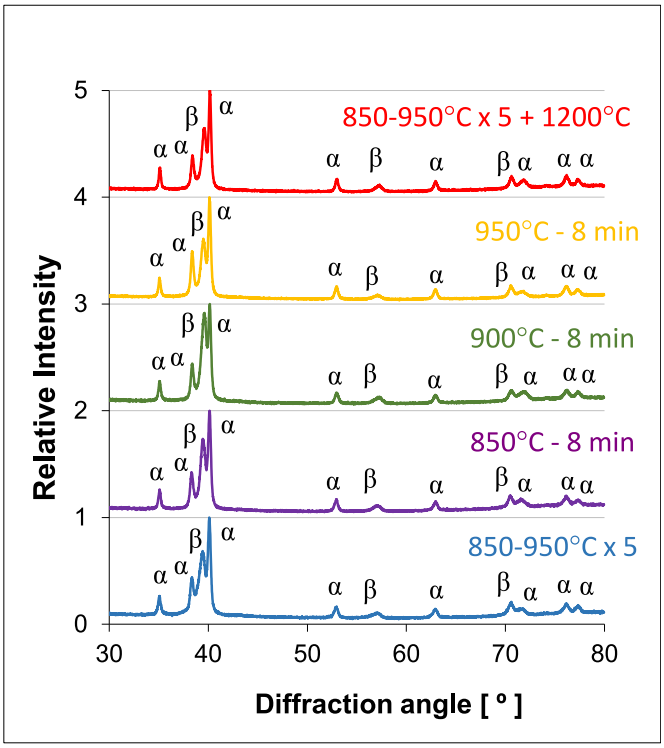

Fig. 9. XRD patterns of the heat-and-hold and cyclic induction sintered Ti-5Fe samples.

achieved by means of the sintering cycle and the associated densification parameter value clearly show that cyclic sintering is beneficial to achieve better densification of the Ti-5Fe samples (Fig. 2). It is eventually found that the actual densification of the induction sintered Ti-5Fe alloy is proportional to the total sintering cycle time, which is an indication of how much time the alloy spends at high temperature (Fig. 2c). It can be argued that extending the holding time at high temperature (e.g., 950 °C) might lead to similar densification values. However, analysis of the data available in literature on induction sintering of the Ti-5Fe induction sintered for a comparable amount of time at slightly higher temperature of this study (i.e., ~1000 °C) [14] yields lower densification and density gain values compared to those of the cyclic sintered alloys of Fig. 2.

From the analysis of the pore structure of the induction sintered Ti-5Fe alloy it is, generally, found that the residual porosity is homogenously distributed in the microstructure with the exception of the alloy sintered using cycle 5 (i.e., 850-950 °C x 4 times +1200 °C). This is because the latter alloy has a slightly less uniform pore distribution with respect to the other alloys. The homogeneous distribution of the pores confirms that a consistent heat distribution within the samples is achieved upon induction sintering. However, the actual sintering cycle has a remarkable effect on the features of the residual pores. Precisely, cycle 1 (i.e., 850-950 °C x 5 times) leads to the formation of pores whose morphology is primarily irregular with a small amount of them having a size greater than 40 μm (Fig. 3). In comparison, the classical heat-and-hold induction sintering cycle generally leads to an overall larger size of the pores with a higher percentage of them being irregular (Fig. 4). However, the increase of the induction sintering temperature is helpful to reduce the overall size of the pores and increase their circularity value (Figs. 5 and 6) achieving comparable pore size and circularity distributions to that of the alloy cyclic sintered between 850 °C and 950 °C. It is worth mentioning that the heat-and-hold induction sintering cycle at 950 °C leads to a more favourable internal pore structure as characterised by a greater number of more rounded pores (Fig. 6c). Finally, cyclic induction sintering with a final heat up to high temperature (i.e., cycle 5) leads to smaller pores with less irregular shape. This general trend is confirmed by the maximum and average pore size as obtained by means of image analysis (Fig. 11a) where it can be seen that both of them decrease with the increase of the induction sintering temperature for the heat-and-hold sintering cycles and smaller pores are achieved using cyclic induction sintering. Additionally, the average circularity of the pores improves with the induction sintering temperature and cyclic sintering is comparable (i.e., cycle 1) or better (i.e., cycle 5), leading to a greater number of almost spherical pores. The values of the relative density of the induction sintered Ti-5Fe samples as calculated via image analysis are consistent with those of the water displacement measurements, although approximately 1 % higher, and so it is the trend where cyclic sintering leads to slightly higher relative density values.

The allotropic phase transformation or β transus of pure Ti (i.e., 882 °C [34]) is oxygen dependent and for Ti grade 2, which has an oxygen content of 0.25 wt%, is 915 °C meaning an upward shift of 33 °C. From the Ti-Fe binary phase diagram [32], the β transus of the Ti-5Fe alloy is meant to be ~800 °C. Estimation of the β transus using the molecular orbital method proposed by Morinaga et al. [35] yields 834 °C. Simplifying and assuming a slightly higher shift on the β transus of the Ti-5Fe alloy due to the purity of the raw materials results in the β transus being ~850-875 °C. As the Ti-5Fe alloy is made using the blended elemental approach, at the beginning of each sintering cycle the densification of the alloy and the dissolution of the Fe powder particles start in the α phase through grain boundary diffusion. When the temperature increases and Fe is effectively dissolved into the Ti lattice the presence of α/β interfaces promotes rapid densification due to volume strain and the defect present in them [26]. The dissolution of Fe also leads to the shifting of the β transus temperature [36]. Consequently, the actual pore structure and its features are determined by the relative position of the specific sintering temperature with respect to the actual β transus of the Ti-5Fe alloy and the maximum sintering temperature used. This is because they dictate whether sintering, or part of the sintering, occurs in the two-phase or single-phase region [37] as time progresses and the Fe atoms are effectively incorporated into the Ti lattice and which diffusion mechanisms are active (Fig. 12). During induction sintering of the Ti-5Fe alloy, surface/grain boundary diffusion and β grain boundary diffusion are active at different stages and the α→β phase transformation and the associated strain, dislocations and interface diffusion play a major role on the densification of the alloy [29]. Combining this theoretical framework with the results of the characterisation of the features of the pore structure (Figs. 3–7) yields that the induction sintered Ti-5Fe samples pass through the initial stage of sintering (i.e., neck formation) and reach the intermediate stage of sintering [38]. In the latter densification, pore rounding, formation of closed pores, and grain growth are expected. It is found that in the induction sintered Ti-5Fe samples different levels of densification and pore rounding occur but the formation of closed pores, and especially grain growth, are rather limited due to the short sintering cycle at relatively low homologous temperatures [39].

The combined SEM (Fig. 8) and XRD (Fig. 9) analyses performed to assess the microconstituents of the induction sintered Ti-5Fe samples confirm that a homogenous composition is achieved regardless of the actual sintering cycle. Specifically, no undissolved powder particles were found during microstructural analysis, EDS chemical analysis results show that the overall distribution of Fe is uniform and consistent with the nominal composition, and no XRD peaks of any phase other than the α and β phases were detected. The achievement of a homogenous chemical composition as such low homologous sintering temperatures, as Ti is most commonly sintered between 1200 °C and 1300 °C [40], is ascribed to the fast sintering kinetics of the induction heating process and it is favoured by the fine particle size of Fe powder used (i.e., <10 μm). The small particle size and the spherical morphology of the Fe powder are ideal as the primary driving force for sintering is the reduction of the overall surface area of the sample, which is enhanced by both aspects [20]. Partitioning of Fe between the α and β phases is found

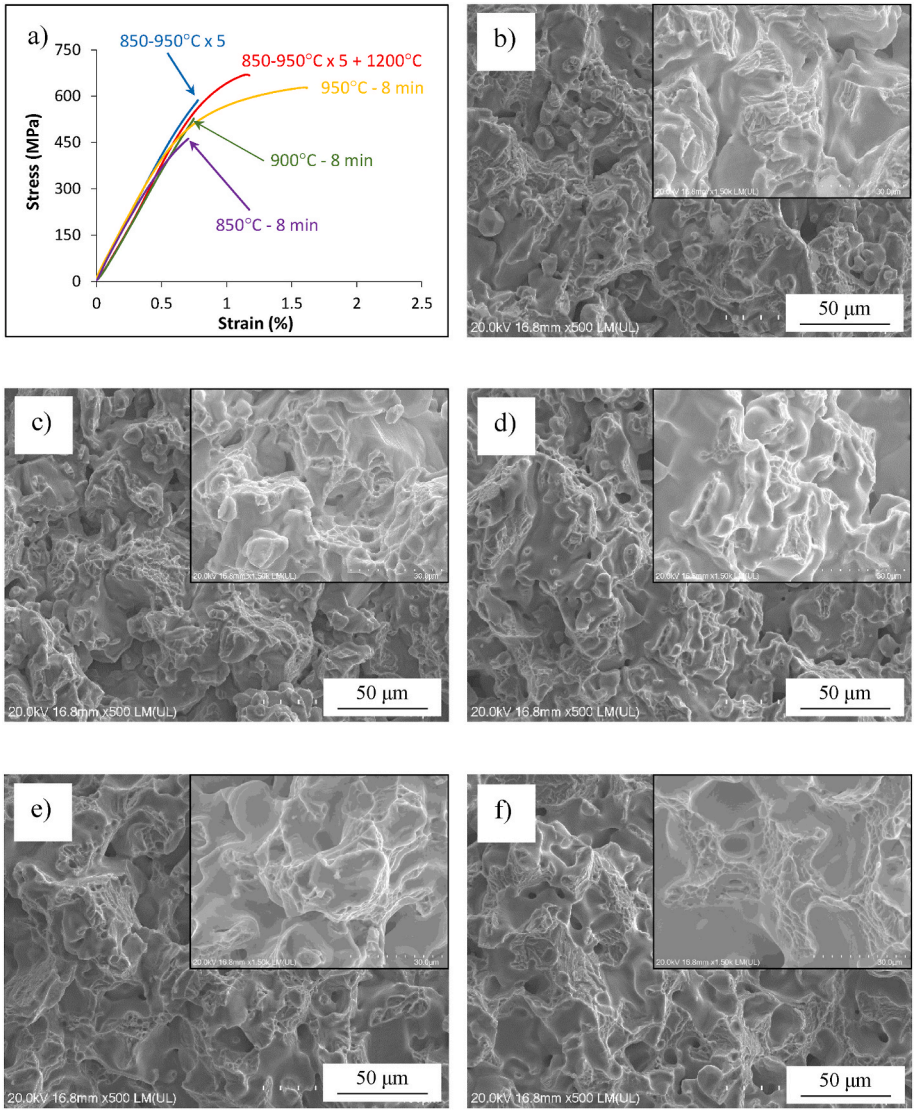

Fig. 10. Results of the mechanical and fractographic analysis of the induction sintered Ti-5Fe samples: a) representative stress vs. strain curves, b) cycle 1: 850-950 °C x 5 times, c) cycle 2: 850 °C - 8 min, d) cycle 3: 900 °C - 8 min, e) cycle 4: 950 °C - 8 min, and f) cycle 5: 850-950 °C x 4 times +1200 °C.

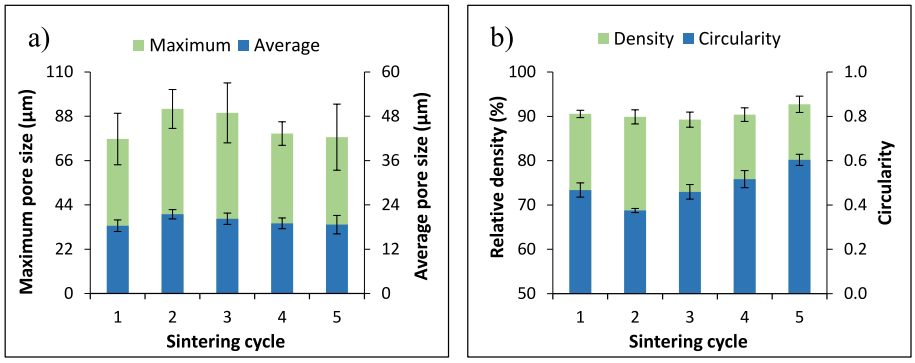

Fig. 11. Average values of the features of the pore structure of the induction sintered Ti-5Fe samples as per image analysis: a) maximum and average pore size, and b) relative density and circularity.

due to the maximum solubility of Fe in these two stable phases. Regardless of the actual induction sintering cycle, the Ti-5Fe samples are characterised by the typical lamellar microstructure of α+β Ti alloys where the lamellae form within the prior β grains upon slow cooling across the β transus temperature. The size of the prior β grains is of comparable magnitude for the different Ti-5Fe samples, and is similar to the powder particle size, due to limited time for grain growth as a consequence of the short sintering cycle and relatively low sintering temperature. The actual induction sintering cycle does have an effect on the features of the lamellar structure (i.e., width of the lamellae) and on

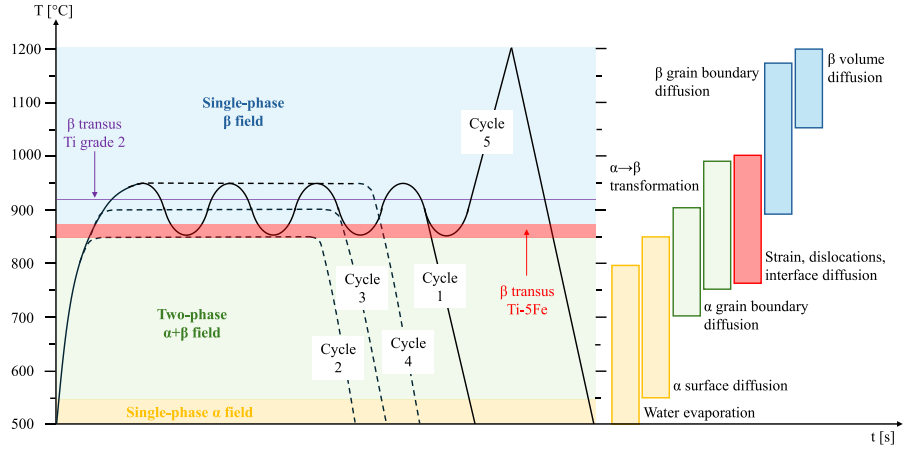

Fig. 12. Sketch showing the relative position of the induction sintering temperature with respect to the β transus of pure Ti (i.e., raw HDH powder), the β transus of the Ti-5Fe alloy, the single- and two-phase fields, and the cascade of events occurring (note: the temperature range for each is only approximate, as adapted from Ref. [26]).

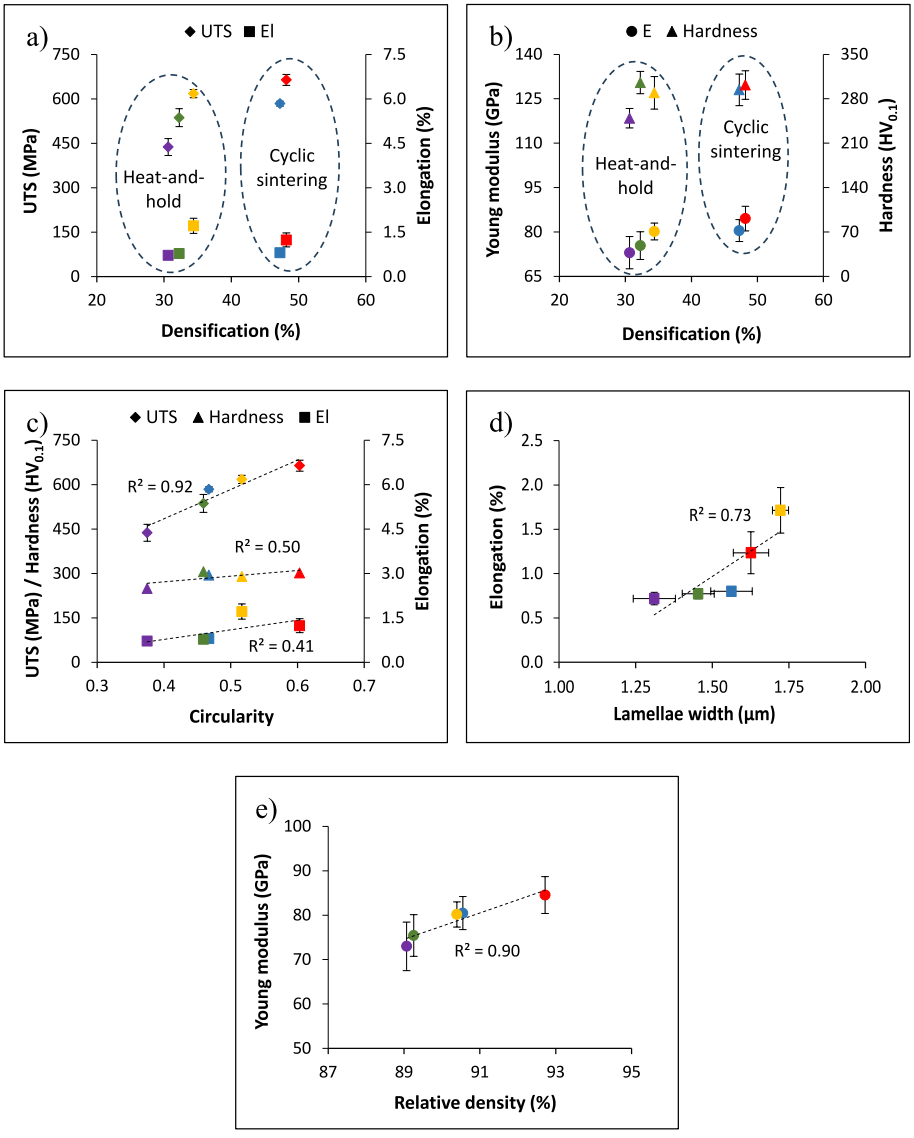

Fig. 13. Average mechanical properties of the induction sintered Ti-5Fe samples: a) ultimate tensile strength and elongation, b) Young modulus and microhardness, c) ultimate tensile strength, microhardness and elongation vs. circularity, d) elongation vs. average lamellae width, and d) Young modulus vs. relative density.

the relative amount of the two phases as per the relative intensity of the XRD peaks. Once again, this is due to the relation of the specific maximum sintering temperature in comparison to the β transus of the Ti-5Fe alloy (Fig. 12). In particular, it is found that the relative intensity of the main peak of the β phase (Fig. 9) is more similar for cycle 1 (i.e., 0.69), cycle 4 (i.e., 0.61), and cycle 5 (i.e., 0.64), but progressively higher for cycle 2 (i.e., 0.74) and cycle 3 (i.e., 0.92), as the actual final sintering temperature influences whether the alloy cools down from above the β transus or within the two-phase region. No significant peaks' position shift or widening was found, but the change in relative intensity is proportional to the actual amount of β phase present in the microstructure and the associated portioning of Fe.

The characterisation of the tensile behaviour of the induction sintered Ti-5Fe samples yields that they mainly deform elastically and are not able to withstand much plastic deformation where both the strength and the elongation increase with the sintering temperature for the heat-and-hold specimens (Fig. 10). On average, the cyclic sintered Ti-5Fe alloy has higher strength but not necessarily higher ductility. Only the Ti-5Fe samples induction sintered using cycle 4 (i.e., 950 °C - 8 min) and cycle 5 (i.e., 850-950 °C x 4 times +1200 °C) undergo enough plastic deformation has to be able to quantify the yield stress by means of the offset method, which is found to, respectively, be 545 ± 25 MPa and 633 ± 19 MPa. The mode of failure of the induction sintered Ti-5Fe samples is primarily related to the propagation of the crack through the residual pores, which having an irregular shape provide an easy pathway for crack propagation. This is consistent with the fairly low ductility of the induction sintered Ti-5Fe samples and it is also found that the amount of ductile zones characterised by the presence of dimples increases with the sintering temperature and the overall sintering cycle time. The analysis of the average mechanical properties of the induction sintered Ti-5Fe samples, which include UTS, elongation, Young modulus, and microhardness, are shown in Fig. 13. It can be seen that, generally, higher performance are achieved for higher densification values, which is expected as this commonly means a lower amount of residual porosity. However, for all the properties, there is a clear distinction as a function of the type of sintering cycle used as the data for the cyclic and heat-and-hold sintering are, respectively, groped together. With the exception of the elongation, the Ti-5Fe samples cyclic sintered 5 times between 850 °C and 950 °C (i.e., cycle 1) have similar properties to those of the Ti-5Fe samples sintered at 950 °C for 8 min. The other heat-and-hold sintering cycles yield lower mechanical performance and the highest are, generally, achieved using cycle 5 (i.e., 850-950 °C x 4 times +1200 °C) although the highest ductility is obtained when using cycle 4 (i.e., 950 °C - 8 min).

A more in-depth analysis of the average performance of the induction sintered Ti-5Fe samples versus the average values of the features of the pore structure obtained through image analysis (Fig. 11) yields that the mechanical properties (i.e., ultimate tensile strength, microhardness, and elongation) correlate better with the circularity (Fig. 13c) rather than the pore size or the relative density. This is coherent with the fractographic analysis which demonstrated that the crack grows by connecting different pores where pores with more irregular shape (i.e., lower circularity value) have a higher stress concentration factor. In particular, it can be seen that the highest correlation (i.e., $R^2 = 0.92$) is found between the ultimate tensile strength and circularity. In the case of the microhardness, due to the small size of the indentation, there is a more pronounced effect from the size of the pores and the microstructural features. Considering the elongation, where the value of the Ti-5Fe induction sintered using cycle 4 (i.e., 950 °C - 8 min) stands out, the lower correlation value found (i.e., $R^2 = 0.41$) indicates a stronger influence from other microstructural aspects (Fig. 8). Therefore, both microhardness and elongation are less dependent on an individual parameter (i.e., the circularity) and their variation is determined by the combination of different microstructural aspects including circularity, pore size, relative density, pore distribution, and features of the lamellar microstructure (e.g., amount of stabilised β phase). It is found that the elongation is better correlated with the average width of the lamellae found within the α+β microstructure (Fig. 13d), rather than the circularity of the pores (Fig. 8d), where lower elongation values are generally found for finer lamellae due to the greater restrain of the movement of the dislocations. Regarding the Young modulus (Fig. 13d), it is found that the highest correlation is actually with the relative density, rather than the circularity, as the stiffness of the sintered alloys is more directly dependent on the total amount of pores present in the microstructure rather than their actual features.

Fig. 14 shows a comparison of the ultimate tensile strength/elongation pairs of the induction sintered Ti-5Fe samples of this study with those of the Ti-5Fe alloy sintered by means of other powder metallurgy methods including induction [14], vacuum [17,41], and microwave [16] sintering without and with further post-sintering thermomechanical processing like hot forging [17] and extrusion [18,19]. It can be seen that the induction sintered Ti-5Fe samples of this study have, in general, comparable properties to literature although they sit at the bottom end of the performance range. This is imputable to the highly irregular pore shape and the associated low relative density values as it can be seen in Fig. 14b) that the strength of the Ti-5Fe alloy monotonically increases with the reduction of the amount of porosity up to the point where the strength is purely dictated by the microstructure for the fully dense (i.e., thermomechanically processed) Ti-5Fe alloy. The main reason for the lower strength or elongation, depending on the specific comparison, is mainly due to the higher sintering temperatures (1110-1300 °C), which determines the final amount of porosity, with respect to the current study. Though, other factors like particle size of the Fe powder, compaction technique used (i.e., cold or warm pressing), and sintering time do also have an effect on the final performance obtained. Fig. 14a) also shows the amount of improvement achievable by subjecting the Ti-5Fe alloy to hot working (i.e., forging or extrusion), which easily double both the strength and the ductility, depending on the selected temperature and amount of plastic deformation applied. Induction

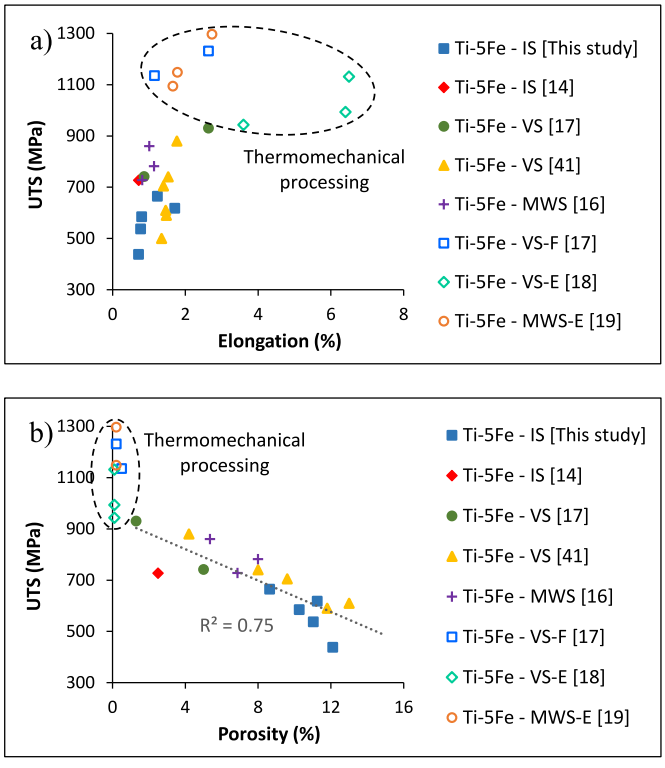

Fig. 14. Comparison of the UTS/elongation pairs of the induction sintered Ti-5Fe samples (a) with literature [14,16-19,41], and (b) variation of the Ti-5Fe as a function of the amount of porosity. Legend: IS – induction sintering, VS – vacuum sintering, MWS – microwave sintering, F – forging, and E – extrusion.

sintering is ideally placed for further post-sintering processing as the thermomechanical deformation can be performed directly on the alloy right after the chosen sintering time has elapsed without the need of reheating the alloy, which is the case when vacuum/microwave sintering or the classical wrought metallurgy route are used. Therefore, if required by the type of application, the performance of the cyclic/heat-and-hold induction sintered Ti-5Fe samples of this study could easily be improved and tailored.

5. Conclusions

This study experimentally compared the yield of cyclic induction sintering to that of the standard heat-and-hold sintering for manufacturing the low-cost Ti-5Fe alloy. From the analysis of the densification response, features of the resulting pore structure, microstructural analysis, and the mechanical performance, the following can be concluded.

- Induction sintering is characterised by very short sintering cycles as a consequence of the exceptionally high heating rates achievable, but this does not preclude the ability to obtain a fully homogeneous chemistry due to the fast sintering kinetics and dissolution of Fe into Ti and it permits to prevent the precipitation of brittle intermetallic phases. The use of low homologous temperatures during induction sintering results in the Ti-5Fe alloy reaching the intermediate stage of sintering and forming the classical lamellar microstructure whose features are mildly affected by the parameters of the sintering cycles investigated.
- Cyclic sintering is beneficial to achieve higher sintering rates as shown by the higher density gain and densification parameter values where the densification of the Ti-5Fe alloy is proportional to the total sintering cycle time and a fairly distribution homogenous of the residual porosity within the microstructure is achieved. The higher densification is ascribed to the cycling through the allotropic $\alpha \rightarrow \beta$ phase transformation. Cyclic sintering also, generally, results in higher relative density, pores with an average and maximum smaller size, and more spherically shaped pores, although these are temperature dependent. Pore size decreases and pores circularity increases with the induction sintering temperature.
- On average, the resulting pore structure of the cyclic sintered Ti-5Fe alloy leads to higher strength but not necessarily higher ductility as most of the samples behaved in a brittle manner as a consequence of the low homologous sintering temperatures. Consequently, the mode of failure is crack propagation through the highly irregular residual pores. Both strength and elongation increase with the sintering temperature for the heat-and-hold sintering cycles and higher performance are achieved when higher densification values are obtained. Pore circularity, rather than relative density, is generally the factor with the highest impact on the mechanical performance of the induction sintered Ti-5Fe alloy combined with the features of the lamellar microstructure (i.e., average lamellae width).

CRediT authorship contribution statement

L. Bolzoni: Writing – review & editing, Supervision, Methodology, Investigation, Formal analysis, Conceptualization. **V. Roduit:** Methodology, Investigation, Formal analysis. **E. Carreno-Morelli:** Supervision, Investigation. **F. Yang:** Methodology. **S. Raynova:** Methodology, Investigation.

Data availability

All metadata pertaining to this work will be made available on reasonable requests.

Declaration of competing interest

The authors declare that they have no known competing financial interests or personal relationships that could have appeared to influence the work reported in this paper.

Acknowledgements

This research did not receive any specific grant from funding agencies in the public, commercial, or not-for-profit sectors.

Data availability

Data will be made available on request.

References

[1] P. Qi, B. Li, T. Wang, L. Zhou, Z. Nie, Microstructure and properties of a novel ternary Ti-6Zr-xFe alloy for biomedical applications, J. Alloys Compd. 854 (2021) 157119.
[2] I. Montealegre-Melendez, E. Neubauer, H. Danninger, Effect of starting powder grade on sintering and properties of PM Titanium metal matrix composites, Powder Metall. 52 (4) (2009) 322–328.
[3] V.A.R. Henriques, P.P. de Campos, C.A. Alves Cairo, J.C. Bressiani, Production of Titanium alloys for advanced aerospace systems by powder metallurgy, Mater. Res. 8 (4) (2005) 443–446.
[4] M. Geetha, A.K. Singh, R. Asokamani, A.K. Gogia, Ti based biomaterials, the ultimate choice for orthopaedic implants - a review, Prog. Mater. Sci. 54 (3) (2009) 397–425.
[5] L. Bolzoni, N.H. Babu, Refinement of the grain size of the LM25 alloy (A356) by 96Al-2Nb-2B master alloy, J. Mater. Process. Technol. 222 (2015) 219–223.
[6] L. Bolzoni, M. Nowak, N. Hari Babu, Grain refining potency of Nb-B -noculation on Al-12Si-0.6Fe-0.5Mn alloy, J. Alloys Compd. 623 (2015) 79–82.
[7] Y. Luo, Y. Xie, Z. Zhang, J. Liang, D. Zhang, Improving strain hardening capacity of high-strength Ti-6Al-4V alloy by a dual harmonic structure, J. Mater. Res. Technol. 26 (2023) 1122–1135.
[8] C. Cui, B. Hu, L. Zhao, S. Liu, Titanium alloy production technology, Market prospects and industry development, Mater. Des. 32 (3) (2011) 1684–1691.
[9] T. Klein, D. Zhang, E. Staufer, T. Boll, C. Schneider-Broeskamp, C. Edtmaier, M. Schmitz-Niederau, J. Horky, D. Qiu, M.A. Easton, Phase transformation pathways in a Ti-5.9Cu alloy modified with Fe and Al, J. Mater. Res. Technol. 27 (2023) 4978–4985.
[10] I. Montealegre Meléndez, E. Neubauer, H. Danninger, Consolidation of Titanium matrix composites to maximum density by different hot pressing techniques, Mater. Sci. Eng. 527 (16–17) (2010) 4466–4473.
[11] P.J. Bania, Beta Titanium alloys and their role in the Titanium industry, J. Occup. Med. 46 (7) (1994) 16–19.
[12] A. Amherd Hidalgo, R. Frykholm, T. Ebel, F. Pyczak, Powder metallurgy strategies to improve properties and processing of Titanium alloys: a review, Adv. Eng. Mater. 19 (6) (2017) 1600743.
[13] M. Koike, C. Ohkubo, H. Sato, H. Fujii, T. Okabe, Evaluation of cast Ti-Fe-O-N alloys for dental applications, Mater. Sci. Eng. C 25 (3) (2005) 349–356.
[14] S. Raynova, F. Yang, L. Bolzoni, Mechanical behaviour of induction sintered blended elemental powder metallurgy Ti alloys, Mater. Sci. Eng. 799 (2021) 140157.
[15] S. Raynova, F. Yang, L. Bolzoni, The effect of thermomechanical treatments on the properties of powder metallurgy Ti-5Fe alloy, Mater. Sci. Eng. 801 (2021) 140389.
[16] S. Raynova, M.A. Imam, F. Yang, L. Bolzoni, Hybrid microwave sintering of blended elemental Ti alloys, J. Manuf. Process. 39 (2019) 52–57.
[17] Y. Alshammari, S. Raynova, F. Yang, L. Bolzoni, Effect of particle size and manufacturing technique on the properties of the PM Ti-5Fe alloy, Int. J. Refract. Metals Hard Mater. 90 (2020) 105246.
[18] C. Romero, F. Yang, S. Raynova, L. Bolzoni, Thermomechanically processed powder metallurgy Ti-5Fe alloy: effect of microstructure, Texture, Fe Partitioning and residual porosity on tensile and fatigue behaviour, Materialia 20 (2021) 101254.
[19] L. Bolzoni, S. Raynova, F. Yang, Work hardening of microwave sintered blended elemental Ti alloys, J. Alloys Compd. 838 (2020) 155559.
[20] S. Germain Careau, E. Ulate-Kolitsky, B. Tougas, In-situ alloying of Ti-5Fe Titanium alloy using direct powder forging and the effect of the powder mixing method, Materialia 24 (2022) 101471.
[21] S. Germain Careau, E. Ulate-Kolitsky, A. Bois-Brochu, Ti-5Fe spherical powder alloy prepared by Electrode induction gas atomization processes (EIGA) for additive manufacturing of biomedical implants, Mater. Lett. 352 (2023) 135238.
[22] H. Wang, H.L. Luo, J.Q. Chen, J.C. Tang, X.Y. Yao, Y.H. Zhou, M. Yan, Cost-affordable, biomedical Ti-5Fe alloy developed using elemental powders and laser in-situ alloying additive manufacturing, Mater. Char. 182 (2021) 111526.
[23] S. Raynova, Y. Collas, F. Yang, L. Bolzoni, Advancement in the pressureless sintering of CP Titanium using high-frequency induction heating, Metall. Mater. Trans. 50 (10) (2019) 4732–4742.

[24] S. Kohara, Effect of repeated allotropic transformation on sintering of Iron powder, Metall. Trans. A 7 (8) (1976) 1239–1241.
[25] K. Akechi, Z. Hara, Increase of sintering rate of Titanium powder during cyclic phase transformation, Powder Metall. 24 (1) (1981) 41–46.
[26] R.M. German, Titanium sintering science: a review of atomic events during densification, Int. J. Refract. Metals Hard Mater. 89 (2020) 105214.
[27] M.T. Jia, B. Gabbitas, L. Bolzoni, Evaluation of reactive induction sintering as a manufacturing route for blended elemental Ti-5Al-2.5Fe alloy, J. Mater. Process. Technol. 255 (2018) 611–620.
[28] X. Zhang, J. Zhou, N. Lin, K. Li, K. Fu, B. Huang, Y. He, Effects of Ni addition and cyclic sintering on microstructure and mechanical properties of coarse grained WC-10Co cemented carbides, Int. J. Refract. Metals Hard Mater. 57 (2016) 64–69.
[29] B. Ye, M.R. Matsen, D.C. Dunand, Enhanced densification of Ti-6Al-4V powders by transformation-mismatch plasticity, Acta Mater. 58 (11) (2010) 3851–3859.
[30] R. Jiang, E. Torresani, A. Maximenko, H. Wang, S. Faulhaber, K. Vecchio, E. A. Olevsky, Cyclic phase transition-assisted spark plasma sintering of AlCoCrFeNi complex concentrated alloys, Metall. Mater. Trans. 55 (4) (2024) 1111–1121.
[31] L. Bolzoni, M. Paul, F. Yang, Effect of combined lean additions of isomorphous and eutectoid Beta stabilisers on the properties of Titanium, J. Mater. Res. Technol. 21 (2022) 3828–3843.
[32] J.L. Murray, Phase Diagrams of Binary Titanium Alloys, first ed., ASM International, 1987.
[33] L. Bolzoni, P.G. Esteban, E.M. Ruiz-Navas, E. Gordo, Mechanical behaviour of pressed and sintered Titanium alloys obtained from prealloyed and blended elemental powders, J. Mech. Behav. Biomed. Mater. 14 (2012) 29–38.
[34] R. Boyer, G. Welsch, E.W. Collings, in: A. International (Ed.), Materials Properties Handbook: Titanium Alloys, Ohio, USA, 1998.
[35] M. Morinaga, N. Yukawa, T. Maya, K. Sone, H. Adachi, Theoretical Design of Titanium Alloys, vol. III, Sixth World Conferecne on Titanium, 1988, pp. 1601–1606.
[36] H. Nakajima, S. Ohshida, K. Nonaka, Y. Yoshida, F.E. Fujita, Diffusion of iron in β Ti-Fe alloys, Scr. Mater. 34 (6) (1996) 949–953.
[37] L. Bolzoni, M. Alqattan, L. Peters, Y. Alshammari, F. Yang, Ternary Ti alloys functionalised with antibacterial activity, Sci. Rep. 10 (1) (2020) 22201.
[38] R.M. German, Sintering Trajectories: Description on how density, surface area, and grain size change, J. Occup. Med. 68 (3) (2016) 878–884.
[39] G. Steedman, S.F. Corbin, J. O'Flynn, Distinguishing the influence of Aluminium and Vanadium additions on microstructural evolution and densification behaviour during the sintering of Ti6Al, Ti4V and Ti6Al4V, Powder Metall. 61 (4) (2018) 301–312.
[40] P.G. Esteban, E.M. Ruiz-Navas, L. Bolzoni, E. Gordo, Low-cost Titanium alloys? Iron may hold the Answers, Met. Powder Rep. 63 (4) (2008) 24–27.
[41] P.G. Esteban, E.M. Ruiz-Navas, E. Gordo, Influence of Fe content and particle size on the processing and mechanical properties of low-cost Ti-xFe alloys, Mater. Sci. Eng. 527 (21) (2010) 5664–5669.